NMR characterisation of dynamics in solvates and desolvates of formoterol fumarate

David C. Apperley, A. Fraser Markwell, Ilya Frantsuzov, Andrew J. Ilott[†], Robin K. Harris and Paul Hodgkinson*

Department of Chemistry, University of Durham, South Road, Durham, U.K. DH1 3LE

* To whom correspondence should be addressed: paul.hodgkinson@durham.ac.uk

[†] Current address: Chemistry Department, New York University, New York, NY 10003, USA

ABSTRACT

Solid-state NMR is used to characterise dynamics in the ethanol solvate of the pharmaceutical material formoterol fumarate and its associated desolvate. Jump rates and activation barriers for dynamic processes such as phenyl ring rotation and methyl group rotational diffusion are derived from 1D-EXSY and ^{13}C spin-lattice relaxation times respectively. ^{2}H and ^{13}C spin-lattice relaxation times measured under magic-angle spinning conditions are used to show that the fumarate ion in the desolvate is undergoing small-amplitude motion on a frequency scale of 100s of MHz at ambient temperature with an activation parameter of about 32 kJ mol^{-1}. Exact calculations of relaxation times under MAS provide a simple and robust means to test motional models in cases where relaxation rate maxima are observed, including for systems where the crystal structure of the material is unknown.

KEYWORDS

Formoterol fumarate, solid-state NMR, solvates, molecular-level dynamics, spin-lattice relaxation, magic-angle spinning

1 INTRODUCTION

The structural characterisation of solid forms that are only available as powders rather than as diffraction-quality single crystals remains a formidable challenge. This is highly relevant to pharmaceutical chemistry where the different solid forms including solvates and hydrates that may be present in production or formulation must be fully understood. A recurring feature is the difficulty of fully characterising forms produced in drying stages by desolvation of solvate forms; such transformations almost inevitably produce fine powders [1]. Although generally crystalline at a local level, the crystallites produced are frequently too small for single-crystal diffraction and may even be too small to give well-defined Bragg diffraction in powder diffraction studies. This inability to characterise desolvates is a serious issue for pharmaceutical chemistry, since desolvation (including dehydration) steps are frequently encountered in production processes.

Formoterol is a rapidly acting and long-lasting β_2-agonist used in asthma therapy as a bronchodilator [2,3], which is generally formulated as its fumarate salt. Figure 1(a) gives its chemical structure and shows the labelling used herein for the carbon nuclei. The forms of formoterol fumarate have been investigated by a variety of techniques [4,5]. Of particular interest here are the isomorphous diformoterol fumarate disolvates, where the solvent is ethanol or isopropanol, and formoterol fumarate form C which is obtained by desolvation of these solvates. The crystal structures of the diethanol and diisopropanol solvates have been determined by single-crystal X-ray diffraction [4], but that of the desolvate form C is not

known: Although powder XRD shows it to be crystalline, crystallites suitable for single-crystal XRD analysis could not be obtained.

Solid-state NMR is a powerful tool for characterising structure and dynamics in molecular solids such as pharmaceuticals [6–12]. Figure 1 shows previously reported [13] ^{13}C spectra of the materials relevant to this work: (b) the CPMAS spectrum of diformoterol fumarate diethanolate, (c) and (d) the CPMAS and "direct excitation" (DE) MAS spectra respectively of form C obtained by desolvation of the ethanolate. The CPMAS spectra readily distinguish the two materials, while the DE spectrum, which highlights ^{13}C resonances with short spin-lattice relaxation times, suggests that the fumarate ion (as well as the methyl groups) are dynamic in the desolvate.

In this work, a variety of NMR experiments is used to characterise the molecular-level dynamics in the desolvate form C, despite its unknown crystal structure. As well as this information being useful in its own right, characterisation of such "dynamic disorder" is a pre-requisite to attempts to solve the crystal structure from powder diffraction studies. Carbon-13 magnetisation transfer experiments allow the dynamics of the phenylene group ring flips to be measured, while ^{13}C spin-lattice relaxation times (T_1) allow methyl group rotation to be characterised. Crucially for structural characterisation, ^{13}C and ^{2}H relaxation times from a sample labelled in deuterium at the CH site in the fumarate ion have been carefully analysed using exact calculations of spin-lattice relaxation times to allow a model to be deduced for the motion of the fumarate ions in the desolvate.

2 EXPERIMENTAL

The diethanol solvate was supplied by AstraZeneca (see Ref. [4] for its preparation), with some excess of solvent to maintain its integrity. Form C was produced by allowing the solvate to dry in air for 2 days [4]. The preparation of selectively ^{2}H-labelled form C is described in Ref. [13].

High-resolution solid-state NMR spectra were obtained using either a Varian Unity Inova spectrometer, operating at 299.82 MHz for ^{1}H and 75.40 MHz for ^{13}C, or a Varian VNMRS 400 spectrometer operating at 100.56 MHz for ^{13}C (399.88 MHz for ^{1}H) and 61.42 MHz for ^{2}H. 7.5 mm (rotor o.d.) and 4 mm magic-angle spinning probes were used on the 300 MHz and 400 MHz spectrometers respectively. High-resolution ^{13}C spectra were recorded under MAS conditions using either cross-polarisation (CP) or direct excitation. The typical CP conditions used were: recycle delay 5 s, contact time 1 ms, acquisition time 50 ms. Spectra were referenced with respect to external neat tetramethylsilane (TMS) for ^{13}C by setting the high-frequency signal from a replacement sample of adamantane to 38.4 ppm.

Variable-temperature measurements of relaxation were performed for form C. Carbon T_1 values were obtained under MAS conditions (spinning rate 6.8 kHz) using the CP-based inversion-recovery method described by Torchia [14], with a contact time of 3 ms. Recovery times ranging from 0.1 s up to 12.8, 25.6 or 102.4 s (as required) were employed, using 7 or 8 increments. Relaxation times were obtained by fitting single exponential decays to signal heights as a function of recovery time. Results (and associated error bars) were averaged where repeat measurements were taken at a single temperature. In most cases, good fits to single exponential behaviour were obtained, with the exception of data measured at estimated sample temperatures above 115 °C; this is close to the melting point of the material, 120–125 °C [4], and so atypical behaviour might be expected. The potential effects of cross-relaxation were investigated by measuring relaxation decays at +30 °C in the presence of a train of 90° ^{1}H pulses (duration 4.2 μs, interpulse delay of 1 ms) during the recovery period.

1D-EXSY / magnetisation-transfer experiments [15] were run on a Varian/Chemagnetics InfinityPlus spectrometer operating at 125.7 MHz for ^{13}C. Samples were packed into 5 mm o.d. magic-angle spinning rotors and measurements taken using a MAS rate of 7 kHz. With the *c*′ peak (115.7 ppm for the ethanolate and 116.9 ppm for form C) on resonance, a fixed t_1 period of 530 μs (ethanolate) or 566 μs (form C) was used to create an initial non-equilibrium state with inverted magnetisation on peak *c* (108.5 ppm for the ethanolate and 109.8 ppm for form C). The magnetisation exchange between *c* and *c*′

resonances was then followed as a function of mixing time, which was actively synchronised with the sample rotation. Data were acquired at 10 °C increments in the range –20 to +40 °C for polymorph C, and from –65 to –5 °C for the ethanol solvate. Repeat data points acquired on cooling confirmed reproducibility. A correction of +3.4 K was made to the set temperatures to correct for the frictional heating of the sample under sample spinning.

^{2}H MAS spectra were acquired at either 46.0 or 61.4 MHz using a 4 mm MAS rotors spinning at 8 kHz. The MAS spectra were fitted to spinning-sideband patterns due to a ^{2}H quadrupole coupling with a Gaussian lineshape function using gsim[16] / pNMRsim[17]. ^{2}H T_1 values were measured as a function of temperature using an inversion-recovery pulse sequence with a shaped adiabatic inversion pulse to improve the efficiency of the inversion (relative to a rectangular 180° pulse). The measurements were obtained using the height of the first rotary echo.

3 ^{13}C SPIN-LATTICE RELAXATION TIMES IN SOLIDS

NMR relaxation times are potentially powerful probes of local dynamics. In particular, spin-lattice (T_1) relaxation times are sensitive to motions at rates of the order of the nuclear Larmor frequency. Moreover, ^{2}H spectra and/or spin-lattice relaxation times are generally very sensitive to modulation of the deuterium quadrupole coupling by motion [18–20]. However, deuterium substitution is not always practical or cost effective. Here we use a combination of ^{2}H (single site) and ^{13}C (multiple site) spin-lattice relaxation time measurements, obtained under high-resolution (MAS) conditions, to build up a picture of the molecular dynamics, focussing on form C for which unusual behaviour associated with the fumarate ion is observed.

There have been numerous studies of methyl group rotation probed via proton spin-lattice relaxation, incorporating low-temperature regimes and quantum tunnelling effects (reviewed by Horsewill [21]). However, there are relatively few literature precedents for the fitting of ^{13}C relaxation data more generally in the solid state, particularly in natural abundance samples. McDowell and co-workers have shown that simple ^{13}C relaxation decays can be observed for polycrystalline samples under MAS, and have extracted site-specific relaxation parameters in several natural abundance amino acids [22,23]. Similarly, site-specific relaxation rates have been measured for the four inequivalent methyl carbon environments in solid L-valine [24]. More detailed information on the local dynamics has been provided by variable-temperature measurements of relaxation as shown for some pharmaceuticals [9], including ibuprofen [25,26], and for methyl α-L-fucopyranose [27] and C_{60} [28].

This sparsity of preceding literature no doubt reflects the relatively low sensitivity of ^{13}C NMR at natural abundance, so many studies of dynamics have used static ^{2}H NMR [18,19] combined with site labelling in order to probe dynamics at specific locations. We show here, however, that ^{13}C relaxation times measured under MAS conditions can provide a convenient way to extract information about the dynamics of multiple sites without the need for specific labelling.

In most cases, ^{13}C relaxation rates resulting from fluctuation of the dipolar couplings between the ^{13}C and neighbouring ^{1}H nuclei are fitted to expressions of the form

$$T_1^{-1}\left(^{13}\mathrm{C}\right) = C\tau_\mathrm{c}\left[\frac{1}{1+\left(\omega_\mathrm{H}-\omega_\mathrm{C}\right)^2\tau_\mathrm{c}^2}+\frac{3}{1+\omega_\mathrm{C}{}^2\tau_\mathrm{c}^2}+\frac{6}{1+\left(\omega_\mathrm{H}+\omega_\mathrm{C}\right)^2\tau_\mathrm{c}^2}\right], \qquad (1)$$

where ω_H and ω_C are the Larmor angular frequencies of ^{1}H and ^{13}C respectively, τ_c is the correlation time for motion and C is a constant which incorporates the magnitude of the dipolar coupling and geometrical factors (notably the "cone angle" of 70.56° in the case of methyl group rotation). Fitting to such expressions involves a number of assumptions. Firstly, that quantum tunnelling effects can be ignored [21,29], which is justified here by the relatively high barriers to motion that are determined below. Secondly, that an expression that is valid for molecules tumbling in isotropic solution is also valid for powder samples under

magic-angle spinning [23,30]. This contrasts to the usual practice in ^{2}H relaxation studies in which non-spinning samples are used and the relaxation rates are typically anisotropic i.e. it is not possible to define a single T_1 relaxation for a powder sample. We confirm below, using exact calculations of relaxation rates, that magic-angle spinning largely removes the orientation dependence of the relaxation rates under typical conditions for ^{13}C NMR. The deviations from simple mono-exponential decays are not significant within the experimental errors.

Finally, the expression above assumes that cross-relaxation effects impact minimally on the observed relaxation rates. In general, in the absence of saturating ^{1}H irradiation during the relaxation period, the decay of ^{13}C magnetisation will be multi-exponential due to heteronuclear cross-relaxation [22,31]. However, such effects would generally have a negligible impact on the elucidated dynamics [32] in cases where the cross-relaxation rate, σ, is small relative to the spin-lattice relaxation rates of ^{1}H and ^{13}C, as long as the ^{1}H polarisation prior to relaxation is consistent between experiments (which is the case when CP is used [14]). Extending the Solomon equations [31] to include continuous ^{1}H irradiation [33], the effect of which can be replicated by a train of 90° pulses [24], shows that the ^{13}C spin-lattice relaxation rate is unperturbed by σ in the limit of strong ^{1}H RF. This was confirmed experimentally by comparing decay curves recorded with and without saturation of ^{1}H spins during relaxation. This was tested at +30 °C, a temperature in the range where the relative contribution of σ is most significant. The differences in the resulting fitted decay constants were within experimental error, justifying the neglect of ^{1}H saturation in subsequent measurements.

Given the limited scope of previous studies, we have performed exact numerical calculations of spin-lattice relaxation rates for different relaxation mechanisms and motional models using the expressions given by Torchia and Szabo [30]. As discussed in Appendix, these expressions express the relaxation rate directly in terms of geometrical factors, such as the cone angle, and the dipolar coupling between ^{13}C and ^{1}H spins at a given orientation. Since the period of the magic-angle spinning (ms) is much shorter than time constants for relaxation (seconds), the mean relaxation rate for a given crystallite can be found by averaging the relaxation rate, R_1, as a function of instantaneous orientation over the rotation period, $\langle R_1(t) \rangle_t$. These average relaxation rates are, in principle, dependent on crystallite orientation (with respect to a frame defined by the rotor axis). In the calculations performed, however, the exact relaxation curve calculated from the weighted sum of the single-exponential decays obtained from different orientations was barely distinguishable from a single-exponential curve with a rate constant obtained from the averaging relaxation rate over the crystallite orientation, Ω, and MAS, $\langle R_1(t) \rangle_{t,\Omega}$. This confirmed the appropriateness of analysing the experimental data from MAS studies in terms of a single, averaged decay constant in the limit that the spinning sideband intensities are small [23,30]. This latter assumption holds well for the ^{13}C results, but not so well for the ^{2}H NMR data (discussed below), where deviations from single exponential behaviour are more marked.

3 ANALYSIS

Evidence for three distinct motional processes was observed in the initial ^{13}C NMR studies of the solvates and the desolvate form C: flips of the phenylene rings, rotational diffusion of the methyl groups, and mobility of the fumarate ion (form C only). These three processes are considered in turn.

3.1 Phenylene ring-flips

As shown in Figure 2, the peaks associated with the aromatic sites *c* and *d* of the formoterol fumarate show changes with temperature that are characteristic [6,34] of relatively

slow (in comparison to the difference in the NMR frequencies) 180° ring flips. Separate lines are seen for the four phenylene CH carbons at low temperatures. Only two lines are observed at higher temperatures, at the average of the low-temperature *c*, *c*′ shifts and separately at the average of the *d*, *d*′ shifts (although this limiting case could not be obtained from the solvates because of the risk of desolvation). The intermediate exchange rate results in coalescence of the resonances for form C and the apparent absence of the phenylene CH signals from the spectra from the solvates.

While these bandshapes can be fitted to extract kinetic parameters, the rates of ring flipping can be determined with much greater accuracy from 1-D EXSY spectra [15]. As described in the experimental section, the *c* and *c*' peak integrals were measured as a function of mixing time; the resulting decays fitted well to single exponentials whose rate constants can be identified directly with ring flipping. Figure 3 shows that the rate constants follow the expected trend for a simple thermally activated process, $\tau_c^{-1} = \tau_0^{-1} \exp(-E_a / RT)$, with the following Arrhenius parameters for the ring flipping dynamics: $E_a = 48.5 \pm 0.7$ kJ mol^{-1}, $\log_{10} \tau_0 = -12.9 \pm 0.2$ for the ethanol solvate, and $E_a = 69.7 \pm 1.6$ kJ mol^{-1}, $\log_{10} \tau_0 = -14.5 \pm 0.3$ for polymorph C. The data confirm the qualitative conclusion drawn from the higher coalescence temperature observed in the form C spectra (Figure 2), namely that the ring-flip motion is significantly more hindered for polymorph C than is the case for the solvates.

3.2 Methyl group dynamics

Figure 4 plots ^{13}C spin-lattice relaxation rates at 100.56 MHz for the two methyl group signals of form C as a function of inverse temperature. There is a clear maximum for the *h* methyl at 1000 K / *T* ~ 4.6 (*T* ~ 217 K) and a less firmly established maximum at 1000 K / *T* ~ 5.0 (*T* ~ 200 K) for the O-methyl. As described above, the relaxation rates were fitted in terms of an exact three-site jump model involving the methyl group geometry (fixed 70.56° cone angle) and the ^{13}C,^{1}H dipolar coupling, D_{CH}, together with a simple Arrhenius-type relationship for the temperature dependence of the correlation rate, $\tau_c^{-1} = \tau_0^{-1} \exp(-E_a / RT)$, which is a good approximation for the limited temperature range observed [21]. The error bars from the fitting of the T_1 values, as shown in Figure 4, were used to weight the data points in the calculation of χ^2 during the fitting of the temperature dependence. The resulting fitted parameters are given in Table 1. Note that the fitting does not take into account uncertainties in the temperature scale due to the effects of the sample spinning. As discussed in the Supplementary Information, the deviation between measured and actual sample temperatures means that the overall uncertainties are somewhat higher. In particular the activation barrier is likely to be underestimated.

Table 1 Parameters from fitting methyl ^{13}C T_1 relaxation rates of Figure 4 to a three-site jump model of methyl group rotational diffusion.

	h methyl	O-methyl
E_a / kJ mol^{-1}	16.0 ± 0.5	16.4 ± 1.0
$\log_{10}$ (τ_0 / s)	–12.5 ± 0.1	–12.9 ± 0.2
D_{CH} / kHz	18.6 ± 0.2	11.4 ± 0.2

The plots show that the data are fitted well, although it should be emphasised that many other models might fit equally well and some care has to be taken in interpreting the results of such modelling. The activation parameters for the two methyl groups are similar and imply that they are relatively hindered [29]. The estimated tunnelling frequency from a potential barrier this size is in the 100s of kHz range, well below the Larmor frequencies involved, justifying the neglect of tunnelling terms to the relaxation [21,35]. This suggests that methyl group "rotation" is a plausible explanation of the ^{13}C relaxation rates. The effective CH dipolar couplings indicate, however, that the model is not perfect. The fitted coupling in the

case of the *h* methyl is somewhat lower than would be expected (about 24 kHz corresponding to a distance of 1.08 Å [36]). This discrepancy may be explained in terms of additional fast motions that reduce the effective dipolar coupling.

The O-methyl relaxation rates are much smaller than those of the *h* methyl. As a result, the fitted effective dipolar coupling is unreasonably small. It could be argued that the R_1 maximum is not clearly defined and could lie at a much higher inverse temperature. However, the slope to low inverse temperature is well established and the deviation of the O-methyl data from this slope at high inverse temperatures can only plausibly be explained by an R_1 maximum; additional relaxation processes would increase rather than decrease R_1. The most straightforward explanation is that the methyl group itself is relatively free to re-orient around the C_b–O bond, leading to a reduction in the effective dipolar couplings. A more involved hypothesis, but one which would explain the similarity of the activation parameters of the two groups, is that two methyl groups are very close in the crystal structure and that the R_1 maximum observed is actually due to the *h* methyl dynamics, while the "true" R_1 maximum associated with the O-methyl dynamics is in a different temperature range.

3.3 Fumarate ion mobility

In order to probe the dynamics of the fumarate ion, ^{2}H NMR spectra and spin-lattice relaxation times were measured in a sample of form C prepared from d_2-fumaric acid. The ^{2}H relaxation time for the labelled polymorph C was found to be significantly faster ($T_1 \approx 30$ ms at 25 °C) than for the starting fumaric acid, which again implies significant mobility. On the other hand, the ^{2}H MAS bandshapes, Figure 5(a), were typical of those obtained from a rigid solid not undergoing any motion, such as that from d_2-fumaric acid, Figure 5(b), and the bandshape from polymorph C showed no significant change over a temperature range from –10 to 80 °C. The quadrupolar parameters obtained by fitting the spinning sideband manifolds were: χ = 160 kHz, η = 0.08 for form C, χ = 169 kHz, η = 0.21 for d_2-fumaric acid, and χ = 168 kHz, η = 0.0 for formoterol fumarate dihydrate, the thermodynamically stable form under ambient conditions (spectrum not shown). As would be expected from the noticeable asymmetry in parts of the experimental sideband patterns [37], the overall quality of fit is not particularly high and statistical error bars (estimated from the residuals) of less than 1 kHz on the χ values should be interpreted with caution.

A couple of limiting models can be proposed to explain the apparent contradiction between the relaxation times, which imply significant rapid motion, and the bandshapes, which suggest that the fumarate ion is static. One solution (model **D**) is that the fumarate is static (or rather not changing orientation), but that the rapid relaxation of the carbon *u* and its associated ^{2}H is *dipolar* in origin and results from close proximity to one of the methyl sites. Another model (**Q**) is that the fumarate ion is undergoing a small amplitude motion, which is large enough to drive ^{2}H relaxation via the modulation of the ^{2}H *quadrupolar* coupling, but without significantly reducing the motionally-averaged χ that would be observed in the bandshape.

Figure 6 plots the rate of spin-lattice relaxation for the fumarate deuterium signal as a function of inverse temperature for models **D** and **Q**. In the dipolar model, the deuterium relaxation is assumed to be driven by three-site jumps of a methyl group. For simplicity, it is also assumed that ^{2}H lies at an equivalent position to the ^{13}C of the *h* methyl group, and the ^{2}H relaxation rate for heteronuclear relaxation between the ^{2}H and the three ^{1}H spins is calculated using the activation parameters derived above for the *h* methyl, adjusting for the different magnetogyric ratio of ^{2}H *vs.* ^{13}C. The resulting estimated rates (dashed line) are clearly too small to make a significant contribution to the relaxation and give an R_1 maximum which is incompatible with experimental data. Moving the position of the ^{2}H would change the overall relaxation rates, but not significantly shift the position of the rate maximum. Clearly, methyl group motion does not explain the ^{2}H results and the modest magnitude of ^{1}H,^{2}H dipolar couplings makes it unlikely that any dipolar mechanism is responsible.

Reverting to the usual assumption that ^{2}H relaxation is driven by modulation of the much larger quadrupolar interaction, the solid line of Figure 6 shows a fit to model **Q** in

which the re-orientation of the C–D bond vector (and hence the principal axis of the ^{2}H quadrupole tensor) can be described in terms of rotational diffusion on a cone – the actual motion is expected to be more complex, but only the re-orientational component is significant here. Assuming that the unknown quadrupole coupling parameters in the absence of motion are similar to those of the dihydrate form, a χ of a 168 kHz and an asymmetry of zero were used to fit the experimental data, together with the methodology described in the Appendix, with the cone angle being a fitted parameter (the cone angle and unaveraged χ are far too strongly correlated to be fitted independently). The fitted parameters for the rotational diffusion rate, D, are E_a = 31.6 ± 1.5 kJ mol^{-1}, $\log_{10} D_0$ = 13.8 ± 0.3 (where $D = D_0 \exp(-E_a / RT)$) and a cone half-angle, Θ, of 10.6 ± 0.6°. The R_1 maximum is not very well-defined and so the D_0 value must be interpreted with care. However, the activation barrier is well-defined and the motion is clearly fast at ambient temperature (D predicted from the fitted parameters is about 100 MHz). In the limit of fast motion on a cone, the quadrupole coupling will be scaled by $(3\cos^2 10.6° - 1)/2 = 0.95$. This is consistent with the marginally smaller quadrupolar parameter χ obtained by fitting the desolvate ^{2}H spectrum, 160 kHz for form C *vs.* 168–9 kHz for samples in which there is no evidence of fumarate mobility.

Note that the relaxation data are not very sensitive to the details of the motional model. For example, relaxation rates were also calculated for a model in which the C–D bond was in symmetrical exchange between two orientations subtending a half-angle of Θ. Although the two-site jump and rotational diffusion models have slightly different functional dependencies, these differences are largely washed out after averaging over MAS and powder orientation. The fitted curve, and fitted parameters, from the two geometrical models were indistinguishable, with the differences lying well within the experimental uncertainties.

This leaves the short relaxation times observed for the fumarate CH (carbon *u*) noted in the direct excitation ^{13}C spectrum, Figure 1(d), to be explained. This situation is only observed for form C, which is consistent with the fumarate ion being relatively mobile in the desolvate. Figure 7 plots the measured spin-lattice relaxation rate as a function of inverse temperature, and compares this with a curve showing relaxation rates calculated on the basis of dipolar relaxation using the motional model and fitted parameters obtained from analysis of the ^{2}H relaxation data, i.e. rotational diffusion on a cone with cone half-angle 10.6°. The value of the ^{13}C,^{1}H dipolar coupling used was 24 kHz (corresponding to a distance of 1.08 Å [36]). Given the absence of fitting parameters, the match between calculated and experimental data is excellent. The only significant deviations are at high inverse temperatures, that is when the relaxation rates are very slow. Such deviations are to be expected since the relaxation rate due to this mechanism is no longer significant and other relaxation processes will start to dominate. Figure 7 confirms that the same model and parameters can be used to explain both ^{13}C and ^{2}H data.

5 CONCLUSIONS

Characterising structure and dynamics in materials where single crystals for diffraction studies are unavailable is a major challenge. While a variety of NMR parameters are sensitive to dynamics on different timescales, it is often difficult to interpret the results obtained in terms of specific motions. Although molecular dynamics simulations are increasingly used to link NMR observations in molecular solids to molecular-level processes [38], such modelling requires an initial structural model. Interpretation of parameters such as NMR relaxation times is especially difficult in the context of heterogeneous and disordered systems, since the dynamic processes are unlikely to be well defined. In contrast, the dynamics of molecular fragments within a crystalline material are expected to be relatively simple, with well-defined correlation times. In these cases it should be straight-forward to calculate relaxation rates as a function of temperature for different models and compare them to experimental data. We have shown that spin-lattice relaxation rates under MAS provide robust estimates of time constants and activation barriers given at least one data set where a relaxation rate maximum is clearly

observed. This allows us to deduce models for dynamic processes, in this case small-amplitude motion of a fumarate ion, even though the structure of the material is unknown. Information on this "disorder" may then be used in attempting to solve the structure of the material from powder diffraction data.

APPENDIX

Table 2: Expressions for spin-lattice relaxation rates due to quadrupolar relaxation (Q) (spin–1) and heteronuclear dipolar relaxation (D) under different motional models from Ref. [30].

Model	Relaxation rate, R_1	Notes
Two-site jump (Q)	$\frac{\omega_Q^2}{8} A_1 \{[B_4 - (0.75B_1 - B_2)\cos 2\phi] g(\tau_c, \omega_I) + [4B_5 - 4B_2 \cos 2\phi] g(\tau_c, 2\omega_I)\}$	$\tau_c = 1/2k$
Three-site jump (Q)	$\frac{\omega_Q^2}{8} \{[A_1B_4 + A_2B_5 - 8A_3B_3 \cos 3\phi] g(\tau_c, \omega_I) + [4A_1B_5 + A_2B_6 + 8A_3B_3 \cos 3\phi] g(\tau_c, 2\omega_I)\}$	$\tau_c = 1/3k$
Free diffusion (Q)	$\frac{\omega_Q^2}{8} \{A_1B_4 g(\tau_{1c}, \omega_I) + A_2B_5 g(\tau_{2c}, \omega_I) + 4A_1B_5 g(\tau_{1c}, 2\omega_I) + A_2B_6 g(\tau_{2c}, 2\omega_I)\}$	$\tau_{1c} = 1/D$ $\tau_{2c} = 1/4D$
Three-site jump (D)	$\frac{9\omega_D^2}{64} \{[A_1B_1 + A_2B_2 + 8A_3B_3 \cos 3\phi] g(\tau_c, \omega_I - \omega_S) + [2A_1B_4 + 2A_2B_5 - 16A_3B_3 \cos 3\phi] g(\tau_c, \omega_I) + [4A_1B_5 + A_2B_6 + 8A_3B_3 \cos 3\phi] g(\tau_c, \omega_I + \omega_S)\}$	$\tau_c = 1/3k$
Free diffusion (D)	$\frac{9\omega_D^2}{64} \{A_1B_1 g(\tau_{1c}, \omega_I - \omega_S) + A_2B_2 g(\tau_{2c}, \omega_I - \omega_S) + 2A_1B_4 g(\tau_{1c}, \omega_I) + 2A_2B_5 g(\tau_{2c}, \omega_I) + 4A_1B_5 g(\tau_{1c}, \omega_I + \omega_S) + A_2B_6 g(\tau_{2c}, \omega_I + \omega_S)\}$	$\tau_{1c} = 1/D$ $\tau_{2c} = 1/4D$

The expressions used to calculate spin-lattice relaxation rates are summarised in Table 2. These involve weighted combinations of correlation functions, $g(\tau_c, \omega) = \tau / (1 + \omega^2 \tau_c^2)$, where τ_c is a correlation time for the process and ω a Larmor angular frequency of the spins involved. The models are: jumps at rate k between two equivalent orientations subtending a half-angle of Θ; rotational diffusion at rate k between three equivalent sites on a cone with a half-angle of Θ; free diffusion on a cone of half-angle Θ. The functions A_1–A_3 and B_1–B_6 which depend on Θ and the polar angles θ, ϕ defining the crystallite orientation respectively are given in Table 2 of Ref. [30]. For quadrupolar relaxation, $\omega_Q = 2\pi\chi$, and for dipolar relaxation

$$\omega_D = \frac{\gamma_I \gamma_S \hbar}{r_{IS}^3} \left(\frac{\mu_0}{4\pi} \right),$$

where r_{IS} is the I,S internuclear distance, and ω_I and ω_S are the Larmor angular frequencies of the ^{13}C and ^{1}H spins respectively (note that the S spin is assumed to be decoupled and saturated).

The relaxation rate can then be calculated for a given relaxation mechanism at a particular instantaneous orientation of the crystallite (defined by θ,ϕ). Since the spinning frequency is much faster than the relaxation rates, the weighting factors can be averaged over the rotor period (30 steps used) and the average relaxation rate for a given powder orientation calculated. Overall relaxation decays, weighted by the spherical polar volume element, were calculated for a powder sample using 30 steps for each of the two polar angles θ,ϕ defining the crystallite orientation. As noted above, these decays were not distinguishable, within the experimental uncertainties, from single-exponential curves with a decay rate calculated from averaging the calculated rate over the polar angles.

ACKNOWLEDGEMENTS

This work was originally supported under EPRSC grant number EP/D057159. IF is supported under EPSRC grant number EP/H023291. Helpful discussions with Prof. A. J. Horsewill (Nottingham) are gratefully acknowledged.

REFERENCES

1. U. J. Griesser, in *Polymorphism in the Pharmaceutical Industry*, ed. R. Hilfiker, Wiley, 2006, ch. 8, pp. 211–233.
2. E. Seberova, A. Andersson, *Respir. Med.*, 2000, **94**, 607.
3. M. Palmqvist, J. Persson, J. Rosenborg, P. Larsson, J. Lötvall, *Eur. Respir. J.*, 1997, **10**, 2484.
4. K. Jarring, T. Larsson, B. Stensland, I. Ymén, *J. Pharm. Sci.*, 2006, **95**, 1144.
5. D. C. Apperley, R. K. Harris, T. Larsson, T. Malmstrom, *J. Pharm. Sci.*, 2003, **92**, 2496.
6. *Solid-State NMR: Basic Principles and Practice*, D. C. Apperley, R. K. Harris and P. Hodgkinson, Momentum Press, 2012.
7. *NMR Crystallography*, ed. R. K. Harris, R. E. Wasylishen and M. J. Duer, Wiley, 2009.
8. M. J. Duer, *Ann. Rep. NMR Spectrosc.*, 2001, **43**, 1.
9. M. Geppi, G. Mollica, S. Borsacchi, C. A. Veracini, *Appl. Spectry. Rev.* 2008, **43**, 202.
10. R. K. Harris, *J. Pharm. Pharmacol.*, 2007, **59**, 225.
11. P. A. Tishmack, D. E. Bugay, S.R. Byrn, *J. Pharm. Sci.*, 2003, **92**, 441.
12. R. K. Harris, *Analyst*, 2006, **131**, 351.
13. D. C. Apperley, A. F. Markwell, R. K. Harris and P. Hodgkinson, *Magn. Reson. Chem.*, 2012, **50**, 680.
14. D.A. Torchia, *J. Magn. Reson.*, 1978, **30**, 613.
15. J. Jeener, B.H. Meier, P. Bachmann, R.R. Ernst, *J. Chem. Phys.*, 1979, **71**, 4546.
16. V. Zorin, *Gsim – a visualisation and processing program for solid-state NMR*, URL: http://gsim.sourceforge.net
17. P. Hodgkinson, *pNMRsim: a general simulation program for large problems in solid-state NMR*, URL: http://www.durham.ac.uk/paul.hodgkinson/pNMRsim

18. *Multidimensional Solid-State NMR and Polymers*, K. Schmidt-Rohr and H. W. Spiess, Academic Press, 1994.

19. R. R. Vold, in *Nuclear Magnetic Resonance Probes of Molecular Dynamics*, ed. R. Tycko, Kluwer Academic Publishers, 1994, pp. 27–112.

20. N. H. M. Hogg, P. J. T. Boulton, V. E. Zorin, R. K. Harris and P. Hodgkinson, *Chem. Phys. Lett.*, 2009, **475**, 58.

21. A. J. Horsewill, *Prog. NMR Spectrosc.*, 1999, **35**, 359.

22. A. Naito, S. Ganapathy, K. Akasaka, and C. A. McDowell, *J. Magn. Reson.*, 1983, **54**, 226.

23. K. Akasaka, S. Ganapathy, C. A.McDowell and A. Naito, *J. Chem. Phys.*, 1983, **78**, 3567.

24. J. Zhou, R. Fu, J. Z. Hu, L. Li and C. Ye, *Solid-State Nucl. Magn. Reson.*, 1997, **7**, 291.

25. E. Carignani and S. Borsacchi and M. Geppi, *J. Phys. Chem. A*, 2011, **115**, 8783.

26. E. Carignani and S. Borsacchi and M. Geppi, *ChemPhysChem*, 2011, **12**, 974.

27. Y. L. Wang, H. R. Tang and P. S. Belton, *J. Phys. Chem. B*, 2002, **106**, 12834.

28. H. He, J. T. Dias, J. Foulkes and J. Klinowski, *Phys. Chem. Chem. Phys.*, 2000, **2**, 2651.

29. M. Prager and A. Heidemann, *Chem. Rev.*, 1997, **97**, 2933.

30. D. A. Torchia and A. Szabo, *J. Magn. Reson.*, 1982, **49**, 107.

31. I. Solomon, *Phys. Rev.*, 1955, **99**, 559.

32. W. Wu, D. L. Noble, J. R. Owers-Bradley and A. J. Horsewill, *J. Magn. Reson.*, 2005, **175**, 210.

33. B. Boulat and G. Bodenhausen, *J. Chem. Phys.*, 1992, **97**, 6040.

34. *Dynamic NMR Spectroscopy*, J. Sandström, Academic Press, 1982.

35. M. Kankaanpää, M. Punkkinen and E. Ylinen, *Mol. Phys.*, 2002, **100**, 2877.

36. F. H. Allen and I. J. Bruno, *Acta Cryst. B*, 2010, **66**, 380.

37. P. M. Henrichs, J. M. Hewitt and M. Linder, *J. Magn. Reson.*, 1984, **60**, 280.

38. A. J. Ilott, S. Palucha, A. S. Batsanov, M. R. Wilson and P. Hodgkinson, *J. Am. Chem. Soc.*, 2010, **192**, 5179.

Figures

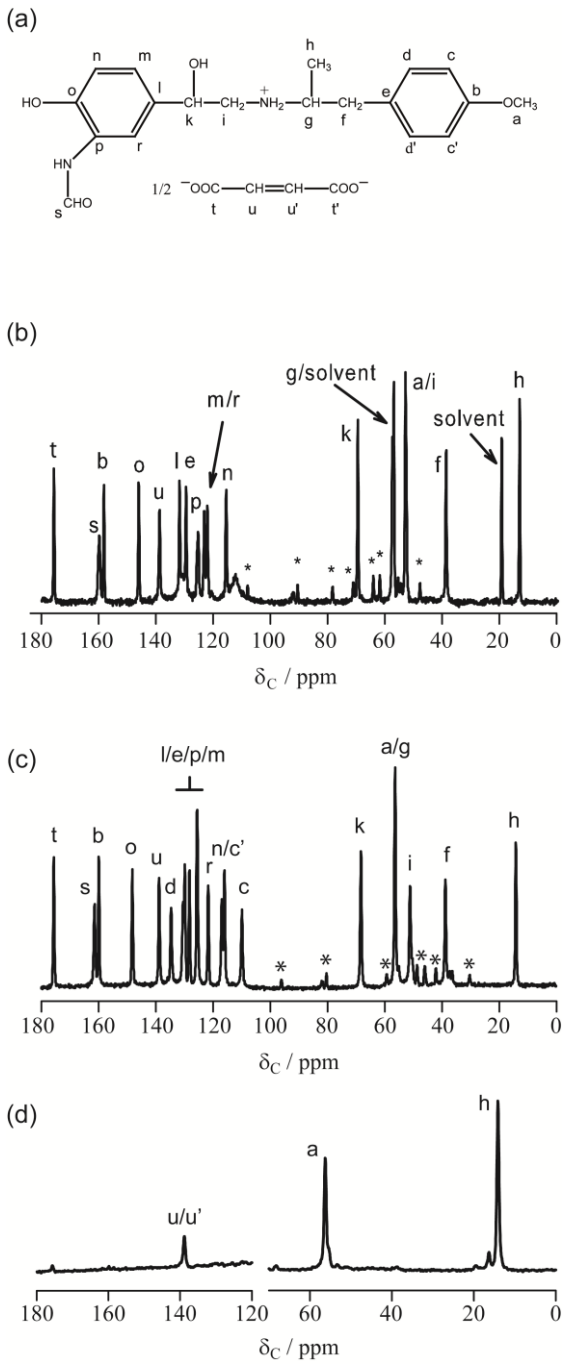

Figure 1. (a) Molecular schematic and carbon numbering for formoterol fumarate. ^{13}C CPMAS spectra acquired at 100.56 MHz of (b) the diethanolate of formoterol fumarate (MAS rate of 6.8 kHz), and (c) form C (MAS rate of 8 kHz). (d) ^{13}C direction-excitation MAS spectrum of form C acquired at 75.40 MHz (MAS rate of 5 kHz) with a recycle delay of 1 s. Spinning sidebands are marked with *.

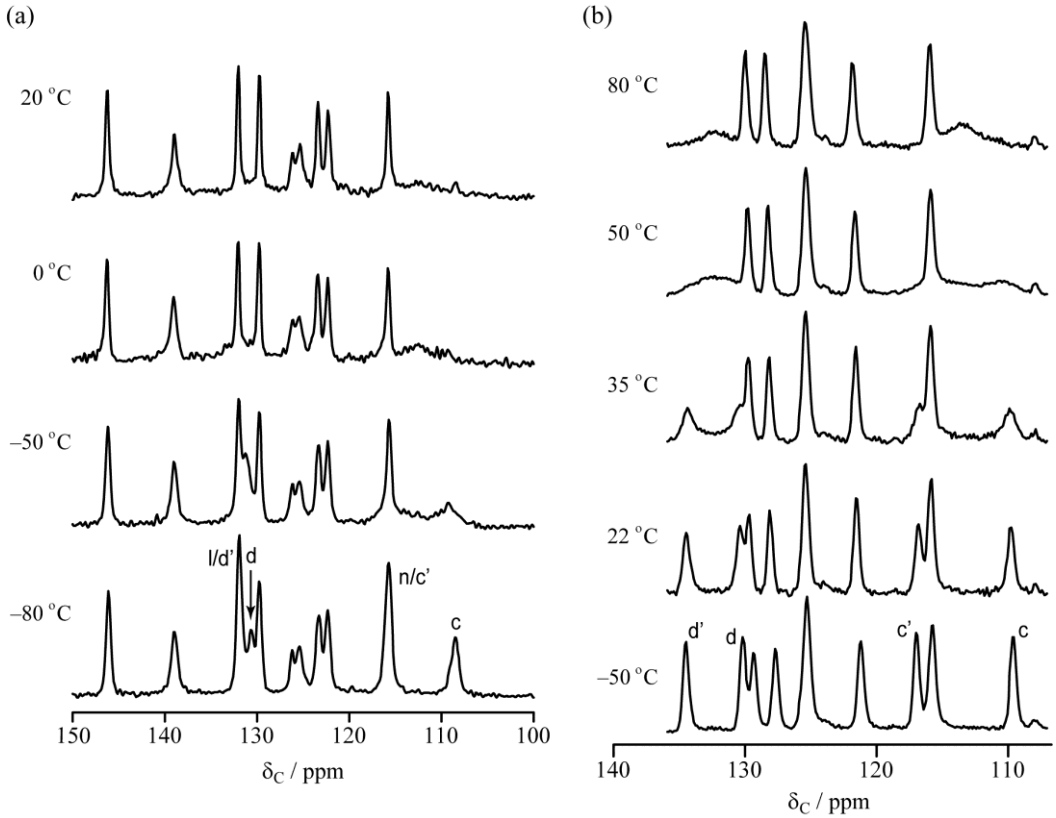

Figure 2. ^{13}C CPMAS spectra acquired as a function of temperature for (a) the diethanol solvate (recorded at 75.40 MHz with an MAS rate of 5 kHz) and (b) for polymorph C (recorded at 100.56 MHz with an MAS rate of 6.8 kHz) showing coalescence of the *c* and *c*' signals between 50 and 80 °C. In (a) the *c*' signal is under the line at 115 ppm and *d*' under that at 132 ppm.

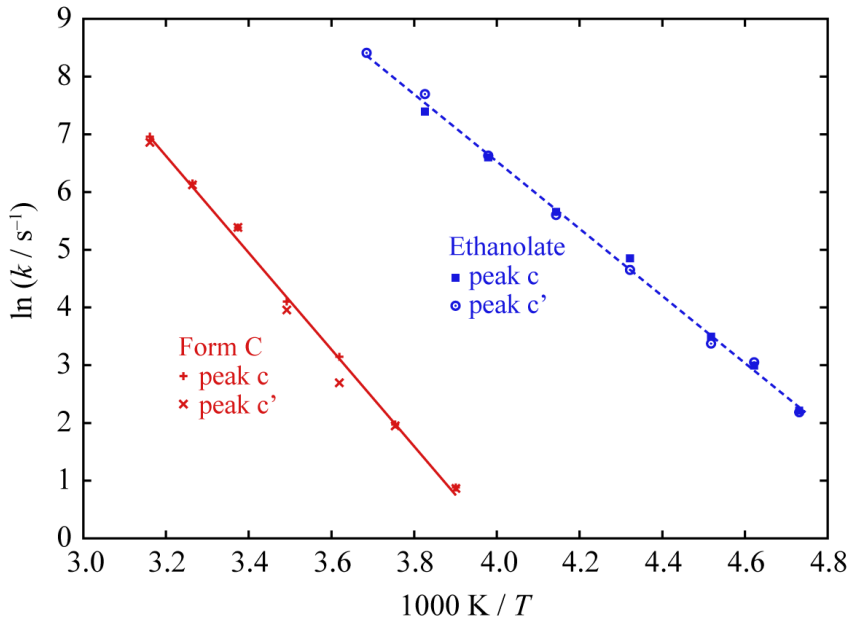

Figure 3. Arrhenius plots of the rates derived from 1-D EXSY experiments on the *c/c'* signals of the phenylene rings of the ethanol solvate and form C. Error bars on individual rate measurements are within the sizes of the points used.

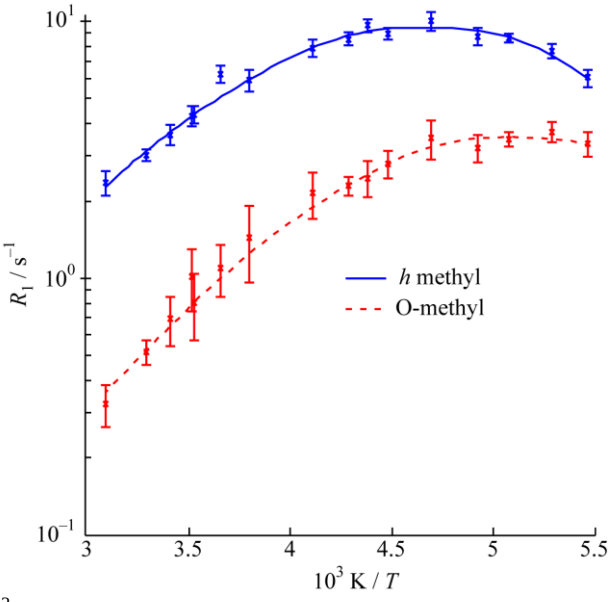

Figure 4. Plot of the ^{13}C spin-lattice relaxation rates (at 100.56 MHz) of the methyl carbons of polymorph C as a function of inverse temperature together with the fits to a three-site jump model.

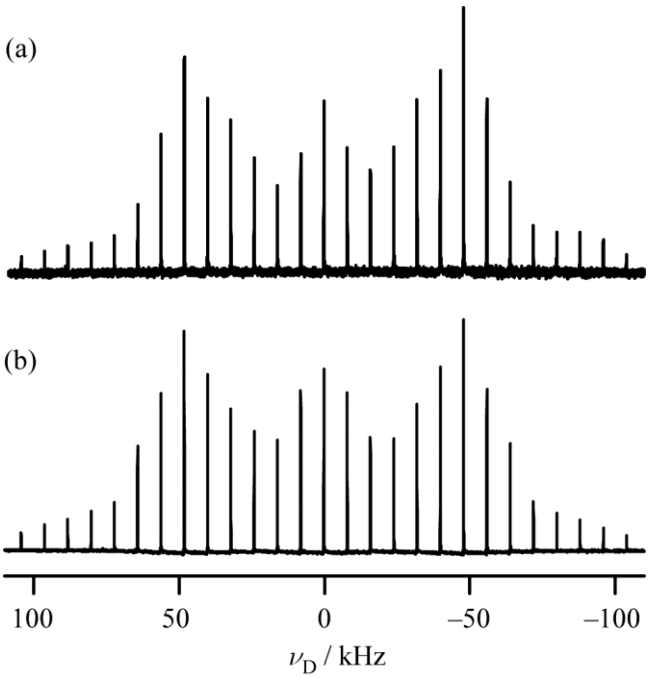

Figure 5. ^{1}H-decoupled deuterium MAS spectra (spinning rate 8 kHz) at ambient probe temperature of (a) form C acquired at 61.4 MHz using direct excitation (2600 repetitions with 1 s recycle delay), (b) d_2-fumaric acid acquired at 46.0 MHz using cross-polarisation from ^{1}H (10 ms contact time, 600 repetitions with 120 s recycle delay). Adapted from data published in Ref. [13].

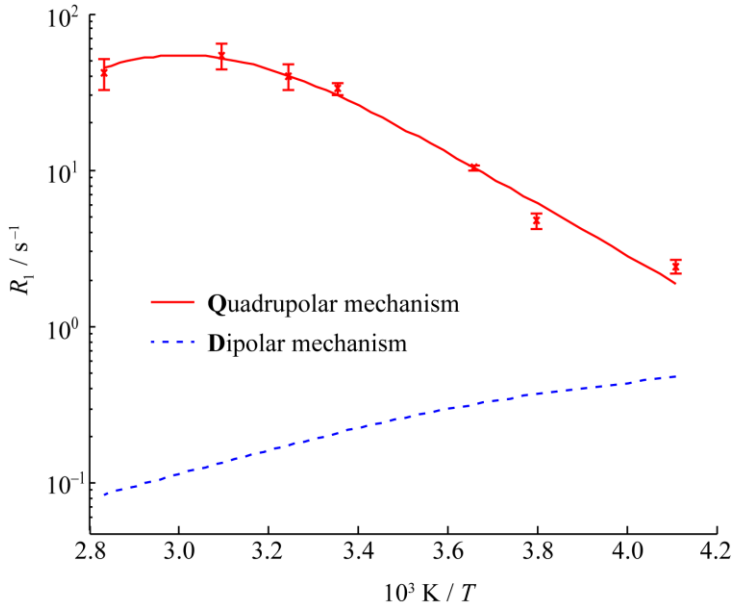

Figure 6. ^{2}H spin-lattice relaxation rates (measured at 61.4 MHz) as a function of inverse temperature for the fumarate CH of form C, and its fit (solid line) to a model of quadrupolar relaxation driven by rotational diffusion on a small-angle cone. The dashed line shows an estimate of the relaxation rate due to dipolar relaxation driven by proximity to a methyl group (activation parameters matching those of the *h* methyl).

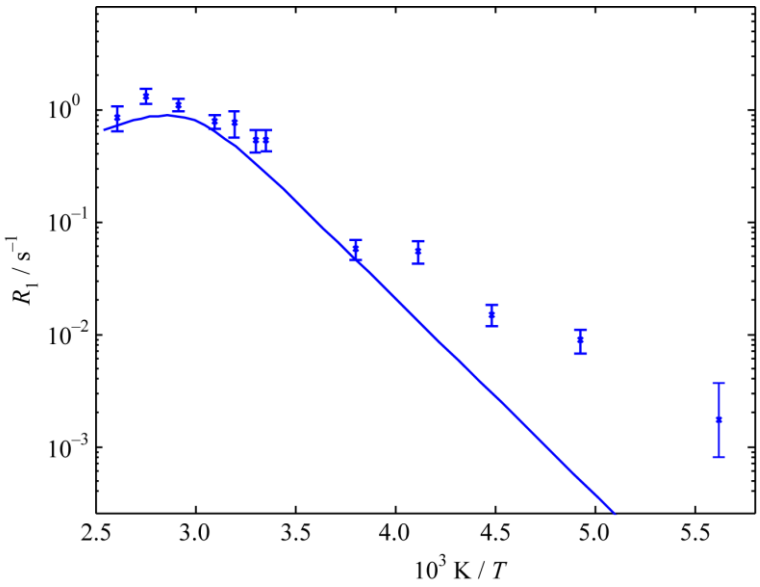

Figure 7. (a) Spin-lattice relaxation rates of the fumarate carbon *u* signal of polymorph C (measured at 100.56 MHz) as a function of inverse temperature; the solid line shows relaxation rates calculated using the motional model of Figure 6.